Etching of the SiGa x N y Passivation Layer for Full Emissive Lateral Facet Coverage in InGaN/GaN Core–Shell Nanowires by MOVPE

Julien Bosch, Pierre-Marie Coulon, Sébastien Chenot, Marc Portail, Christophe Durand, Maria Tchernycheva, Philip Shields, Jesús Zúñiga-Pérez, Blandine Alloing

Etching of the $SiGaN_x$ passivation layer for full emissive lateral facet coverage in InGaN/GaN core-shell nanowires by MOVPE

*Julien Bosch *†, Pierre-Marie Coulon †, Sébastien Chenot †, Marc Portail †, Christophe Durand ‡, Maria Tchernycheva ◊, Philip A Shields•, Jesús Zúñiga-Pérez†§, Blandine Alloing †*

†CRHEA-CNRS, Rue Bernard Gregory, 06560 Valbonne, France

‡Univ. Grenoble Alpes, CEA, Grenoble-INP, IRIG, PHELIQS, NPSC, 38000 Grenoble, France

◊Centre de Nanosciences et de Nanotechnologies (C2N), Univ. Paris-Saclay, Boulevard Thomas Gobert, 91120 Palaiseau, France

• University of Bath, Claverton Down, Bath, United Kingdom

§MajuLab, International Research Laboratory IRL 3654, CNRS, Université Côte d'Azur, Sorbonne Université, National University of Singapore, Nanyang Technological University, Singapore, Singapore

Authors to whom correspondence should be addressed: julien.bosch@crhea.cnrs.fr

KEYWORDS: Core shell nanowire, GaN, wet etching, dry etching, cathodoluminescence, quantum well, underlayer.

Abstract

To strongly enhance the vertical growth rate in MOVPE-grown GaN core-shell wires, large quantities of silane (SiH_4) need to be introduced during the growth of the wire core. This results in the formation of a $SiGaN_x$ layer that acts effectively as a dielectric mask on the sidewalls of the GaN core, thereby promoting the vertical growth. While useful during core growth, its presence precludes the formation of homogeneous core-shell heterostructures, whose coverage and optical quality tend to be maximized at the top of the wires. In this paper, we propose three different strategies to remove this passivating layer once its initial role accomplished. They are based on either chemical, physical or thermal etching. Their effect in the optical quality of subsequent core-shell InGaN/GaN heterostructures, including single and multiple-quantum well heterostructures, has been analyzed. Overall, an *ex-situ* chemical etching of $SiGaN_x$ by H_3PO_4 results in an enhanced emissive coverage and a stronger overall luminescence intensity from the active regions, while simultaneously removing deep-defect emission arising from the high growth temperature of the core.

Introduction

InGaN/GaN heterostructures are a material of choice for their applications in fields such as, but not limited to, lasers[1,2], lighting[3,4], and displays[5]. In this context, the growth of planar nitride heterostructures has been documented for more than 25 years[6,7]. However, because of the polarity of GaN, the growth of heterostructures along the *c*-axis leads to the so-called Quantum-Confined Stark Effect (QCSE), in which the quantum well (QW) band structure is distorted by the internal

polarization fields, leading to a decrease in the wavefunction overlap between electrons and holes. The QCSE is responsible for the power dependence of the wavelength of the emitted light, for the reduction of the overall efficiency and for longer carrier lifetimes (which could be beneficial in the absence of omnipresent non-radiative defects)[8]. To overcome these problems, one way is to grow QWs on non-polar GaN planes. One possibility that does not require expensive non-polar GaN substrates is to grow nanowires (NWs) along the *c*-axis and directly use the non-polar $\{1\bar{1}00\}$ *m*-plane sidewalls to grow the QWs. This "core-shell" structure also presents the advantage of having fewer or no dislocations (thanks to dislocation bending[9,10,11] and mask filtering[11,12] in the case of selective area growth). The high structural quality of the core and the absence of QCSE allows the growth of an InGaN shell with a larger thickness, reducing thereby the efficiency droop for a given light emission intensity thanks to the need of a reduced current density[13,14]. The last advantage of the nanowire geometry is that with proper aspect ratios and spacing, the emissive surface is larger than that of standard planar LEDs.

Two main growth techniques, i.e. pulsed growth mode and continuous-flow mode have been reported for the growth of GaN nanowires by Metal-Organic Vapor Phase Epitaxy (MOVPE) and the impact of the growth parameters have been analyzed[15,16,17,18]. In the case of continuous flow mode, temperature and V/III ratio appear as key parameters to promote GaN growth along the c axis[17,18]. However, when playing with these parameters, GaN nanowires height is usually limited to few microns (1-3 µm). In order to significantly increase the vertical growth rate and reach >10 µm height nanowires, large quantities of SiH_4 must be introduce into the reactor [10,19,20,21,22,23]. The introduction of SiH_4 during MOVPE growth leads to the formation of a thin passivation layer of $SiGaN_x$ on the lateral facets of the wires[24] as reported by Tessarek et *al.*[25]. This layer acts as a dielectric mask and promotes the diffusion of the reacting species along the sidewalls up to the top

of the wire thus highly enhancing the vertical growth[23,25]; the second effect is the enhanced doping of the GaN core, which is beneficial for subsequent core-shell LEDs fabrication[26]. The presence of this $SiGaN_x$ layer has since then been evidenced in several other reports[22,27,28,29,30,31,32,33,34,35]. Unfortunately, this passivation layer impacts the structural and optical quality of the InGaN shell grown on it by degrading the sticking of species and the resulting morphology[27,31]. To avoid this issue, often the core growth is finished by a "non-intentionally doped" (nid) GaN portion during which SiH_4 is no longer introduced in the reactor[28,30,36]. The surface of the nid GaN is thus not covered by the $SiGaN_x$ passivation layer. When the active InGaN shell region is subsequently grown, the shell covers only the top nid part of the wire, which limits the overall light emitting area[25,30]. In addition, the active region grown in the top part can be strongly degraded by a defective ultra-thin $SiGaN_x$ underlayer, due to the residual SiH_4 in the reactor chamber[30].

Another method to circumvent the negative effect of the $SiGaN_x$ layer consists in burying it. One possibility is to use AlGaN as an underlayer before the growth of the LEDs active region, given its ability to nucleate on $SiGaN_x$[28,36]. However, while AlGaN underlayers have been used previously for reducing leakage current[37,38] and for burying defects and optimizing crystalline quality[39,40], only few reports show a successful increase of the InGaN QWs intensity at the NW base[41]. Besides, AlGaN can also lead to cracks in the shell,[28,36] as reported in the case of N-polar GaN NWs. Similarly, a GaN layer grown at low temperature reduces the Ga atom mobility and therefore enhances similarly the nucleation on top of the $SiGaN_x$ layer, thus burying it. Still this method does not allow full emissive coverage[30], and very few articles, one to our knowledge, show a luminescence along the entire length of the nanowires grown by continuous MOVPE[41].

In this report, we propose another approach that consists in removing completely this $SiGaN_x$ passivation layer by a chemical or physical treatment[23,27,29], exposing the whole non-polar facet of

the NW and hence enabling full emissive coverage of the wire by the subsequent InGaN shell. This paper investigates first the impact of the treatment on the InGaN shell: we show that the luminescence of a single QW can be enhanced depending on the chemical or physical treatment. Second, the effects of these treatments on the surface of the underlying GaN are studied through the growth of a sample with an InGaN underlayer and a sample with three QWs. This provides a first understanding of the effects of the tested treatments on the GaN material quality and how it translates to the quality of the shell heterostructure. Last, a study of the emission on the entire length of the nanowire was realized, showing a clear impact on the emissive coverage of the treatments.

Experimental Section

The NWs were grown using selective area growth (SAG) on a GaN template grown on *c*-plane sapphire substrate covered with a 35 nm thick SiO_2 mask deposited by PECVD. The pattern on the mask was fabricated using Displacement Talbot lithography and inductively coupled plasma etching[42], resulting in openings with a diameter of 300 nm and a pitch of 1.5 µm. The SAG of NWs was performed in a MOVPE Thomas Swan showerhead reactor with 1790 µmol/min NH_3 and 110 µmol/min Trimethylgallium (TMGa), giving a low V/III ratio of 15 typical of NW growth. Silane was added during the whole core growth at a flux of 0.4 µmol/min. Other growth parameters were as follows: a setpoint temperature of 1175°C, a pressure of 100 Torr, a growth time of 1800 s and a carrier gas ratio of $H_2/N_2 = 3$. In total, six identical samples were obtained. One of them is kept as reference while the others are used for the following experiments.

Three kinds of treatments have been investigated to remove the $SiGaN_x$ layer: wet etching, dry etching and thermal etching. For wet etching, 3 different chemical solutions have been tested. Diluted Buffered Oxide Etch (BOE), potassium hydroxide (KOH)[43] and phosphoric acid (H_3PO_4)[44] have been chosen as they were all reported to etch $SiGaN_x$. Moreover, KOH is able to etch GaN, especially N-polar *c*-planes and semi-polar planes[45,46,47,48]. H_3PO_4 was also reported to etch semipolar planes in GaN NWs[29,48,49,50]. More precisely Deeb et *al.*[29] showed by a surface photovoltage measurements that H_3PO_4 treatment removes the surface states and reveals bulk-like properties of the underlying GaN. The exact protocols were as follows: The BOE was diluted 80 times, and the sample was treated for 10 seconds at room temperature. The KOH etching was performed with 45% KOH at 75°C for 5 minutes. Last, the H_3PO_4 etching was realized with 85% H_3PO_4 at 125°C for 10 minutes. Regarding the dry etching, one sample was treated using reactive ion etching in an Oxford system 100 ECR-RIE apparatus with SF_6 at 200W for 20s. Last, a method avoiding taking the samples out of the growth reactor was tested, and consisted in using an *in-situ* annealing under H_2 only at 1175°C for 15 seconds as a method of thermal etching.

After the treatments, the samples were reintroduced in the MOVPE reactor for the shell growth. Three different shell structures were grown and are represented on figure 1. For each sample, the regrowth started by growing a spacer of GaN at 1175°C during 100s with NH_3 and TMGa fluxes being respectively 0.13mol.min^{-1} and 55µmol.min^{-1}. A first structure containing one single InGaN quantum well (SQW) was grown on all the samples at 850°C and 100 Torr during 360s. The NH_3, TMGa and Trimethylindium (TMIn) fluxes were 0.13mol.min^{-1}, 58µmol.min^{-1} and 32µmol.min^{-1}, respectively, with N_2 as the carrier gas. QWs were subsequently capped using a layer of GaN grown at 1060°C, under the same fluxes for NH_3 and TMGa, and without any TMIn introduction. The second series contained a shell structure made of an InGaN underlayer (UL) followed by a

single QW. The underlayer was grown at 880°C and 100 Torr for 600s. The precursor fluxes were the same as for the QWs except for TMIn, which had a reduced flux of 18µmol.min^{-1}. A third series of shell structures containing three QWs (MQWs) was also fabricated. The QW growth conditions were the same for all structures. A summary of all samples highlighting the different treatments and the regrown shells is given on table 1. For simplicity, the samples will be referred by the nature of the treatment to which they were exposed (reference, SF_6, H_3PO_4, KOH, BOE, H_2 annealing), as well as the shell structure used (SQW, UL+SQW, MQW). Last, the emission properties of the samples were measured at room temperature using a scanning electron microscope (SEM) equipped with a cathodoluminescence (CL) setup, operated at 5kV and with a constant probe current of 5.4nA.

Results and discussion

Single Quantum Well (SQW). SEM images of the NWs have been taken systematically before and after the shell deposition in order to monitor the effects of the treatment and assess the shell quality, as depicted in figure 2. The morphology of the NWs in the SF_6 and BOE treated sample (figure 2b and 2e) is similar to the reference sample (figure 2a), which indicates that any effect of the treatments should be localized close to the top surface. In the case of both H_3PO_4 (figure 2c) and KOH (figure 2d) treatments, a smoothing of the edges between neighboring non-polar facets as well as between the lateral non-polar and the top semi-polar facets is observed. Further, in the case of H_3PO_4 the top part of the sidewalls at the edges between *m*-plane facets seems to have been etched (which is more visible for a longer time of etching, as seen in **Supporting information S1**). Last, in the case of the H_2 annealing (figure 2f), the top surface has been thermally etched

away while the lateral non-polar facets seem unaffected, suggesting that in these conditions GaN is preferentially etched compared to the $SiGaN_x$ passivation layer. Images at much larger magnification of a layer around the GaN core (**Supporting information S2**) suggest a $SiGaN_x$ thickness of around 25nm, which is much thicker than the $SiGaN_x$ layer reported by Tessarek et *al*.[25]. This could mean that this layer might contain some GaN that stayed unetched by the treatment.

Figures 2(g) to (l) show the morphology of the NWs after the subsequent growth of the SQW shell. The reference sample (figure 2g), i.e. without $SiGaN_x$ removal, shows a high surface roughness on both the lateral *m*-planes, due to the direct nucleation on the $SiGaN_x$ layer, and the topmost semipolar planes, which display an inhomogeneous and uncomplete coverage. On the other hand, the SF_6 SQW sample (figure 2h) displays relatively smooth *m*-plane facets, with a minor growth disruption on the top *c*-plane of the truncated pyramid. This suggests that the surface of the core has been modified by the etching treatment. A similar result can be seen with the H_3PO_4 SQW sample (figure 2i), with a smooth and continuous *m*-plane, suggesting an extended emissive coverage. The NWs on the KOH SQW (figure 2j) sample have a "match-head" shape and some visible roughness at the edges between the *m*-plane facets, just below the "match-head". This is consistent with the smoothing of the upper part of the wires after KOH treatment, suggesting that the QW containing shell has only been deposited on the top part of the wire. The BOE sample (figure 2k) shows similar rough features at the edges between the *m*-plane facets but with a covering of the shell being more homogeneous in thickness along the wire. Finally, the H_2 SQW samples (figure 2l) shows a high roughness on the *m*-plane facets, similar to the reference sample, and a clear overgrowth of a pyramid on the top part of the wire. This confirms the assumption that

only the upper part of the NWs consisting of the semi-polar plane facets was etched away by the H_2 treatment, while the $SiGaN_x$ layer survives the H_2 treatment.

Figure 3a shows cathodoluminescence (CL) measurements made at room temperature on a single representative NW for each sample. These spectra have been obtained by integrating the emission spectra of hyperspectral images along the entire NW length. Four emission bands can be identified. The first one, around 364nm, is attributed to the GaN band edge. The red shifted emission compared to bulk GaN has already been reported in the case of VLS-grown Si-doped GaN NWs[51]. This phenomenon has already been studied in Si-doped planar polar *c*-plane[52] and non-polar *a*-plane[53] GaN and could be explained by both bandgap narrowing and tensile strain introduced by the Si atoms[54]. The second is a large band centered at around 550nm, identified as the yellow band [55,56,57]. Finally, two other emission bands centered at around 400nm and 450nm can be identified and attributed to the InGaN QW luminescence. The 400nm band is generally identified as the *m*-plane luminescence from the QW, while the 450nm band is caused either by the red-shifted luminescence of *r*-planes QWs, or by In-rich clusters at the junctions between *m*-planes, which will be further discussed later in this document.

The GaN band edge signal is visible on all the samples and in particular for the reference sample and H_2 SQW sample. However, the luminescence peak at 400nm is observed only on the H_3PO_4, SF_6 and KOH SQW samples. The signal at 450nm is visible on all samples except for the BOE sample, whose general luminescence intensity is very weak. On the contrary, a strong luminescence is observed on the H_2 SQW sample but it is largely due to the emission of the yellow band. Finally, the H_3PO_4 sample shows the strongest luminescence at 400nm and a much weaker YB emission as compared to all other samples.

CL maps at 400nm and 450nm (figure 3b) allow to visualize the spatial distribution of these emission bands along the whole NWs length and, thus, evaluate the impact of the treatment on the shell's light emission. Some small disparities in height can be observed in SEM images and CL maps, which may be due to size inhomogeneity but more likely to the manual method used to remove the nanowires from their host substrate which does not guarantee to cut them precisely at their base. It should be noted that the intensity of the CL maps is arbitrary, and one should refer to figure 3a for a quantitative intensity comparison between the samples. In particular, monochromatic hyperspectral maps at 400nm allow to illustrate the efficiency of the employed treatment to grow a radiative SQW on *m*-plane sidewall facets. Note that a similar reasoning could be applied to the monochromatic images at 450nm, though the conclusions could be misleading due to the strong contribution of the yellow band, even at this wavelength, for some of the samples.

One should note first that for the reference, BOE and H_2 SQW samples, the intensity at 400nm is very low compared to all other three samples (figure 3a,b) and, thus, they can be excluded from the following analysis. Interestingly, while the signal at 400nm for the other samples is comparatively strong, its spatial distribution is very different: SF_6 and H_3PO_4 samples clearly display a SQW emission extending over the topmost half of the NWs, while in the KOH treated NWs the SQW emission comes preferentially from the top 0.75µm of the nonpolar planes, which is consistent with the SEM observations (fig 1j).

Moreover, the CL maps in figure 3b show different origins for the emission at 450nm. Indeed, reference, SF_6 and H_2 SQW samples shows a 450nm emission coming from the top pyramidal part of the wire with no signature detected on the non-polar sidewalls. Semi-polar planes are known to incorporate more indium[58], which has already been observed in NWs. The higher intensity observed for the H_2 SQW sample could be explained by the larger surface of the pyramid

overgrown at the top of the wire (see figure 2(l)). For the three other samples, the emission at 450nm is more evenly distributed along the non-polar facets. A remarkable point concerns the H_3PO_4 sample: indeed, the 450nm signal is coming from the edges between *m*-plane facets and its spatial distribution is complementary to the emission at 400nm. One hypothesis is that the 450nm emission is due to a greater incorporation of indium on the edges, which has been previously detected and ascribed to a combination of strain relaxation occurring at the edges[59] along with the formation of nanometric *a*-plane facets[60,61]. Another explanation could be that H_3PO_4 etches preferentially the *a*-planes over *m*-planes in GaN, which is supported by a recent study on etching barrier index calculations[50], as introduced in Ref 47 to approximately predict relative resistance to etching of each crystallographic plane. A similar conclusion could be made for the top of the KOH SQW sample, but not for most of its sidewall. Indeed, a consistent 450nm signal is visible on the whole sample, despite no 400nm emission. Several explanations could be at play here (inhomogeneous etching leading to inhomogeneous emission, impurities introduced by the KOH, etc…), but it is difficult to conclude on the precise origin of this behavior. Last, the BOE sample also seems to exhibit 450nm emission from the sidewalls, but this emission can be ascribed to the tail of the yellow luminescence band of the sample as suggested by the corresponding spectrum on figure 3a.

These measurements evidence the impact of the treatments on the shell luminescence efficiency and on its coverage: measurements on the reference sample clearly show that the regrowth of the InGaN shell on the $SiGaN_x$ passivation layer results in an excessive amount of defects, which prevents any QW emission from *m*-plane sidewalls. Similarly, BOE etching or H_2 annealing do not give satisfactory results. On the other hand, a more homogeneous distribution of the shell is obtained by chemical treatment with SF_6, KOH and in particular H_3PO_4. This last chemical

treatment allows a strong enhancement of the CL emission while reducing the YB emission, which suggests a better structural quality and, potentially, less incorporation of deep defects.

Effect on heterostructures containing InGaN underlayer (UL) and multi quantum well (MQW) samples. It has been shown in Ref 62 that in the case of planar GaN grown at a temperature higher than 900°C some point defects appear in the GaN and segregates at the surface. According to the authors, this defect could be a nitrogen vacancy (v_N) that would form non-radiative centers in quantum wells by reacting with In. One way to solve the problem is to grow a so-called "underlayer" (UL) with a small In composition below the QWs in order to bury these defects[63]. This result is further supported by the fact that it is possible to observe the defects accumulating in the first quantum well in samples with MQWs[64]. However, most reports on this subject focus on *c*-plane planar GaN and similar studies on core-shell structures are scarce. Among them, Kapoor et *al.*[30] observed that an UL with indium seemed to have no effect on the efficiency of the QW. In this section different core-shell structures have been studied to evidence the effect of etching treatment on the potential point defects associated to a defective GaN surface layer.

Both SQW+UL and MQW structures were grown on reference, SF_6 and H_3PO_4 samples. The choice of these two last samples among others described in the previous section, along with the reference sample, is motivated by the fact that they are the most luminescent samples. In addition, these two chemicals are known to attack the materials differently, because the SF_6 is expected to etch only the $SiGaN_x$ passivation layer, while H_3PO_4 is expected to also etch the GaN core. The UL was chosen with a low-In content InGaN in order to compare the results with the literature[30]. The spatially-integrated spectra are given in Figure 4 and a CL-mapping of a representative NW

of each sample is also provided in Figure 5. The CL spectra and maps presented for the SQW samples in both figures are the same as the ones presented in figure 3 and were included for comparison.

In the case of the reference sample, an increase of one order of magnitude of the QW peak is observed with the addition of an UL. On the other hand, the intensity of the MQWs sample is comparable to the one of the UL sample, but redshifted by 50 nm. The CL-mapping shows that the UL sample is the only one that exhibits *m*-plane luminescence.

For the SF_6 treatment, the 400nm peak associated with the *m*-plane QW emission is noticeable on every sample, and along a significant part of the wire, which is a signature of the $SiGaN_x$ passivation layer. Here again, the addition of an UL results in an increase of one order of magnitude of the luminescence intensity. A threefold increase can be noticed with the use of several QWs.

Last, the samples treated with H_3PO_4 behaves differently. First, on the SQW spectrum, the dominant emission is the 450 nm band and, as shown on figure 4, it comes from the entire length of the NW. Second, the UL addition does not increase the 400 nm *m*-plane emission, however, a suppression of the emission at 450nm can be noticed. In the MQW sample, the intensity of the 400 nm peak is increased by one order of magnitude.

The results will now be discussed more in depth, and an explanation to the observed phenomena will be provided. Regarding the reference sample, a comparable luminescence increase is observed with respect to the SQW case both on the UL and on the MQWs samples. One possible explanation is that this improvement is due to the burial of non-radiative centers; in the first case (MQWs) it would be achieved by the addition of QWs, the first QWs being used to bury the non-radiative centers without providing further intensity, while in the second case it would be achieved by the

addition of an UL which traps defects, but also increases the emissive coverage on the *m*-plane of the NW, resulting in an intensity similar to the one in the MQW sample. Lastly, no QW emission can be seen at wavelengths shorter than 450 nm, whereas most other samples have an *m*-plane QW signal at 400 nm. The SQW+UL sample also exhibits some interesting *m*-plane luminescence, which is further discussed in **Supporting Information S3**.

For the SF_6 sample, the same mechanism is at play, and confirms that there is a defect responsible for non-radiative centers in the QW that can be suppressed by the addition of an underlayer. However, as said before, the luminescence of the MQWs sample here is greater than the one with the underlayer, which is expected since one can roughly consider that the first QW buries or traps the defects, and the second and third one contributes effectively to the overall emission, thus resulting in a total intensity larger than that of just one QW. This contrasts with the reference sample, where the first two QWs seem to be needed to bury the non-radiative centers[64], which is consistent with a higher defect density (see Figure 2g). It is important to note that the obtained results seem contradictory with the ones obtained in Ref. 30, in which the combination of an UL with a GaN spacer appears to have no effect on the luminescence intensity. A possible explanation is that the residual $SiGaN_x$ ultra-thin layer on the wire sidewalls reported in the Ref. 30 can trap the point defects and prevent any diffusion into the shell. The subsequent spacer growth is realized at a temperature of 900°C, which is the low temperature threshold for point defect formation[62].There are therefore few or no defects trapped in the UL. In the present case, since the $SiGaN_x$ layer has been etched, the point defects are free to diffuse in the shell, even at low shell growth temperature. An underlayer may therefore be required to achieve a satisfactory luminescence in NWs where the core passivation layer has been removed.

The behavior is different for the H_3PO_4 samples. First, the addition of an UL results in a disappearance of the 450nm emission. This could be explained by the fact that the growth rate of the *a*-planes responsible for the emission at this wavelength in the H_3PO_4 SQW is faster than that of *m*-planes so that the *a*-planes disappear during the UL growth[65], resulting in the 400nm GaN *m*-plane emission being the only emission measured in the SQW+UL sample. A weak 450nm shoulder can be noticed in the spectrum of the MQW sample and is visible on the fig 4c which could be due to an emission from the first QW. Second, while the UL is expected to trap non-radiative centers and thus to increase the luminescence intensity, as seen in the two other samples, this is not the case here. One possible explanation for this is the etching of the GaN by the H_3PO_4. According to Ref. 62, the defects responsible for non-radiative centers are segregated at the surface, and their incorporation in bulk GaN is negligible. On the other hand, it has been observed in Ref. 29, that a short H_3PO_4 treatment on GaN nanocolumns made them exhibit bulk-like properties. An interpretation of the result presented in this study is that the H_3PO_4 has been able to etch the surface of the GaN, and particularly the surface defects responsible for non-radiative centers. The UL thus no longer plays its role as an NRC trap, which explains why no intensity increase can be noticed. On the other hand, the MQW sample has a more intense 400nm signal because all the QWs are free of NRC-inducing surface defects and contribute to the overall intensity. It can also be noted that, if the three MQW samples are compared, the intensity of SF_6 and the control sample are similar, while the H_3PO is almost four times more intense.

Emissive coverage of the MQW samples after SF_6 and H_3PO_4 treatments. Finally, in order to attest the relevance of our approach for the realization of LED devices based on core-shell nanostructures, we extracted the CL spectra of SF_6 and H_3PO_4 MQW samples at the top; bottom

and middle of the NW (figure 6). It is noteworthy that the luminescence signal is still clearly visible until the NW base where the intensity is comparable to that of the yellow band. Note that the yellow band intensity remains constant all along the nanowire. This result is significantly better than the ones found in the literature[30,31,40], where the luminescence coming from the quantum well usually collapses near the middle of the nanowire. It demonstrates that our approach allows us to obtain a full shell luminescence on doped nanowire grown by continuous MOVPE. Both H_3PO_4 wet etching and SF_6 dry etching thus appear to be efficient and easy processes to completely etch the $SiGaN_x$ layer.

Conclusion

This paper explores strategies to etch away the $SiGaN_x$ layer covering the lateral facets of heavily Si-doped GaN NWs grown by MOVPE in order to achieve a full InGaN shell emissive coverage along the entire NW length and to improve its optical quality. Except for the BOE treatment, all samples showed an improved intensity of the *m*-plane QW luminescence as compared to the untreated fully doped NW. Among all the treatment performed, SF_6 dry etching and H_3PO_4 chemical etching appear to be the most promising ones in order to efficiently remove the SiGaNx layer and thus, to extend the InGaN shell luminescence along the entire NW length. In addition, through the comparative study of different InGaN shell structures, we suggest that the H_3PO_4 treatment not only remove the SiGaNx layer but also some GaN core surface defects. Finally, the study of the SF_6 and H_3PO_4 treated samples' luminescence along their whole length highlights a dramatic increase of the MQW's emissive coverage, confirming that fully covered core shell NWs

can be obtained through SiGaNx etching processes. This significant increase of the luminescence signal suggests that SiGaNx removal by etching is a very promising method for improving the efficiency of core-shell nanowire LEDs.

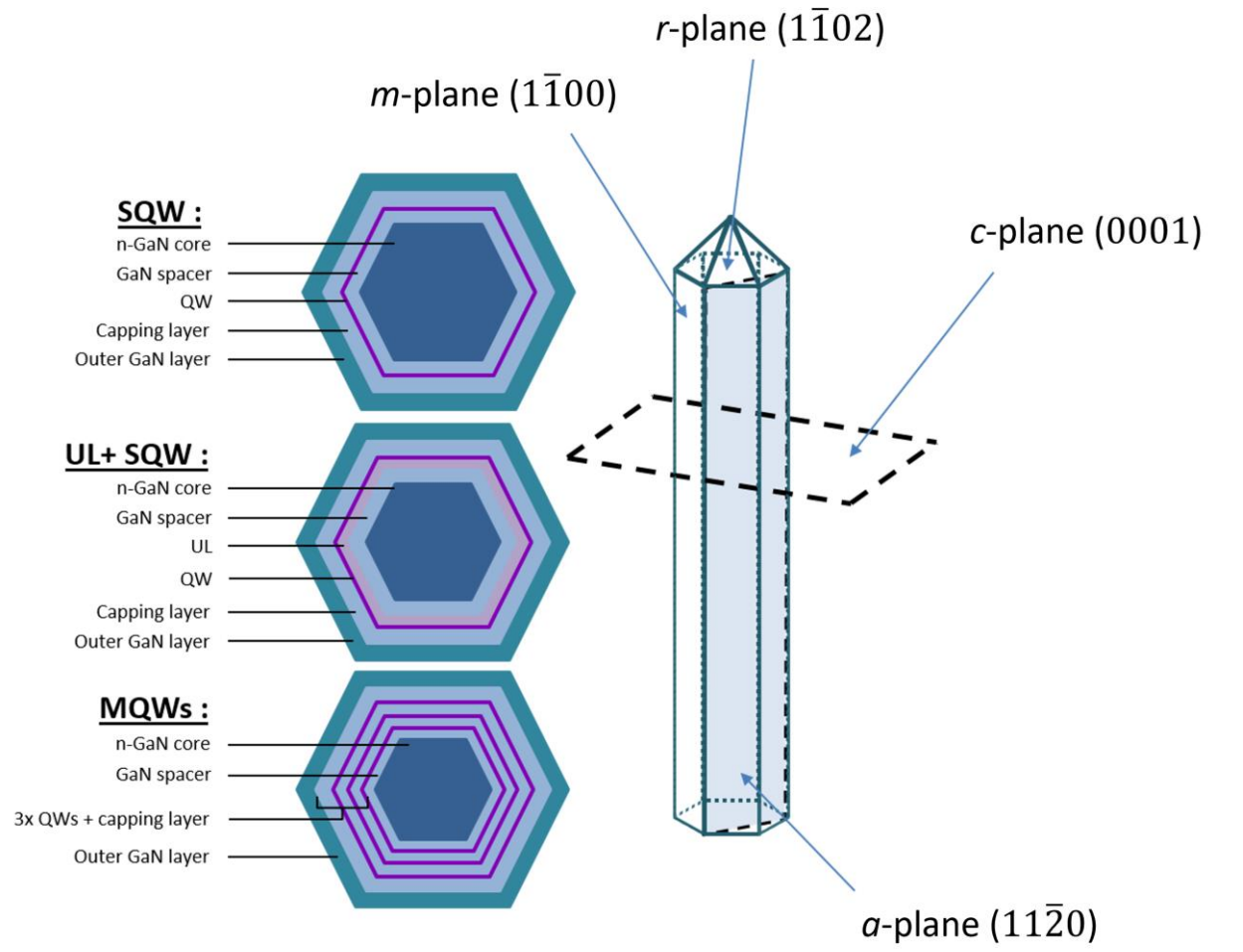

Figure 1. Structure of the three different shells and critical crystallographic planes in GaN nanowires

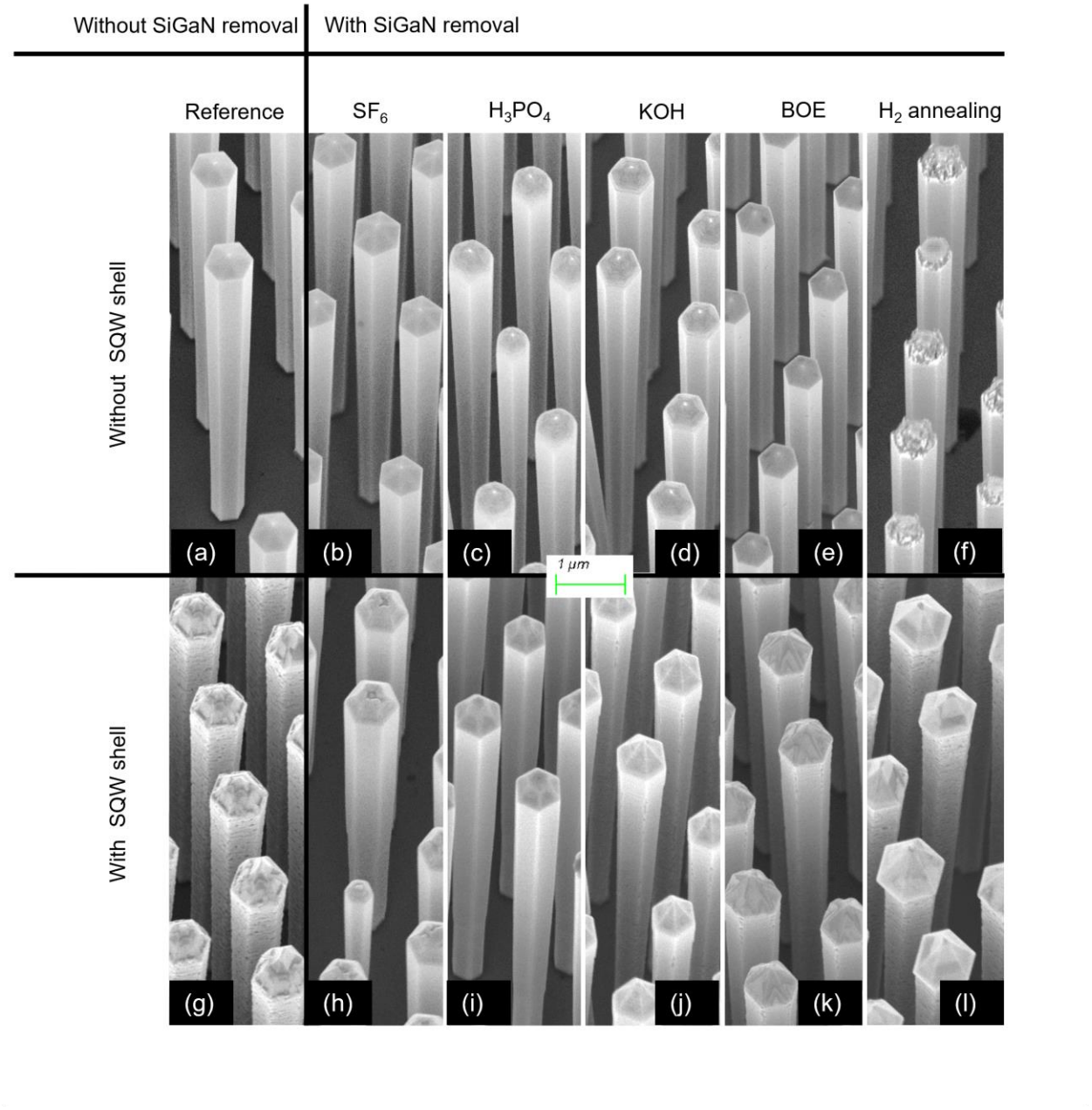

Figure 2. SEM images with 25° tilted view of: (a) to (f), doped core NW after surface treatment, and (g) to (l), the same samples after a subsequent shell growth

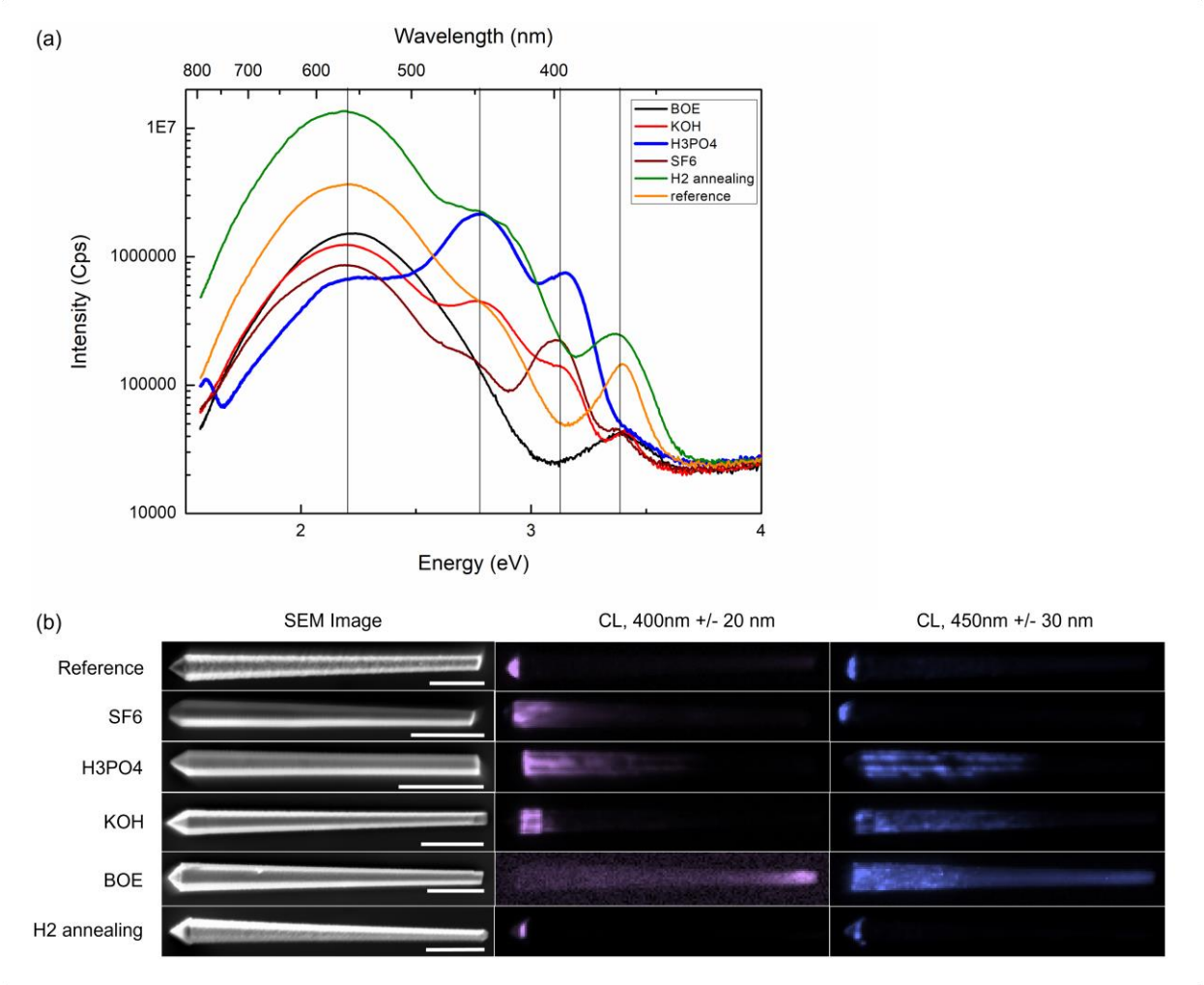

Figure 3. (a) CL spectra of SQW samples for treated and untreated samples. CL spectra were generated from the hyperspectral data set by adding the spectra of each pixel of the map, thus corresponding to the overall emission of the nanowire from top to bottom. The curve for H_3PO_4 has been highlighted as it is the best performing sample in this test. (b) SEM images of the NWs and corresponding normalized CL map of the luminescence intensity at 400 +/- 20 nm (c) and 450nm+/-30nm (d). The scale bars are 2µm.

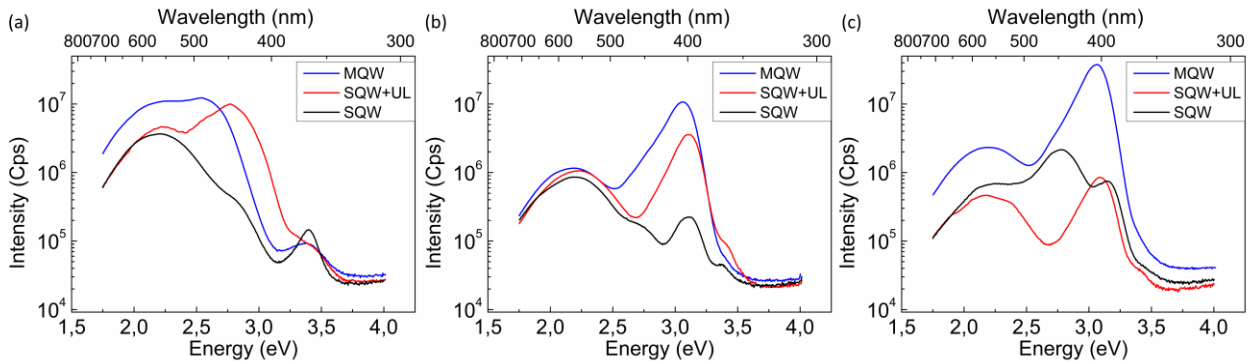

Figure 4. CL spectra for untreated (a), treated with SF_6 (b) and treated with H_3PO_4 (c) samples. CL spectra were generated from the hyperspectral data set by adding the spectra of each pixel of the map, thus corresponding to the overall emission of the nanowire from top to bottom.

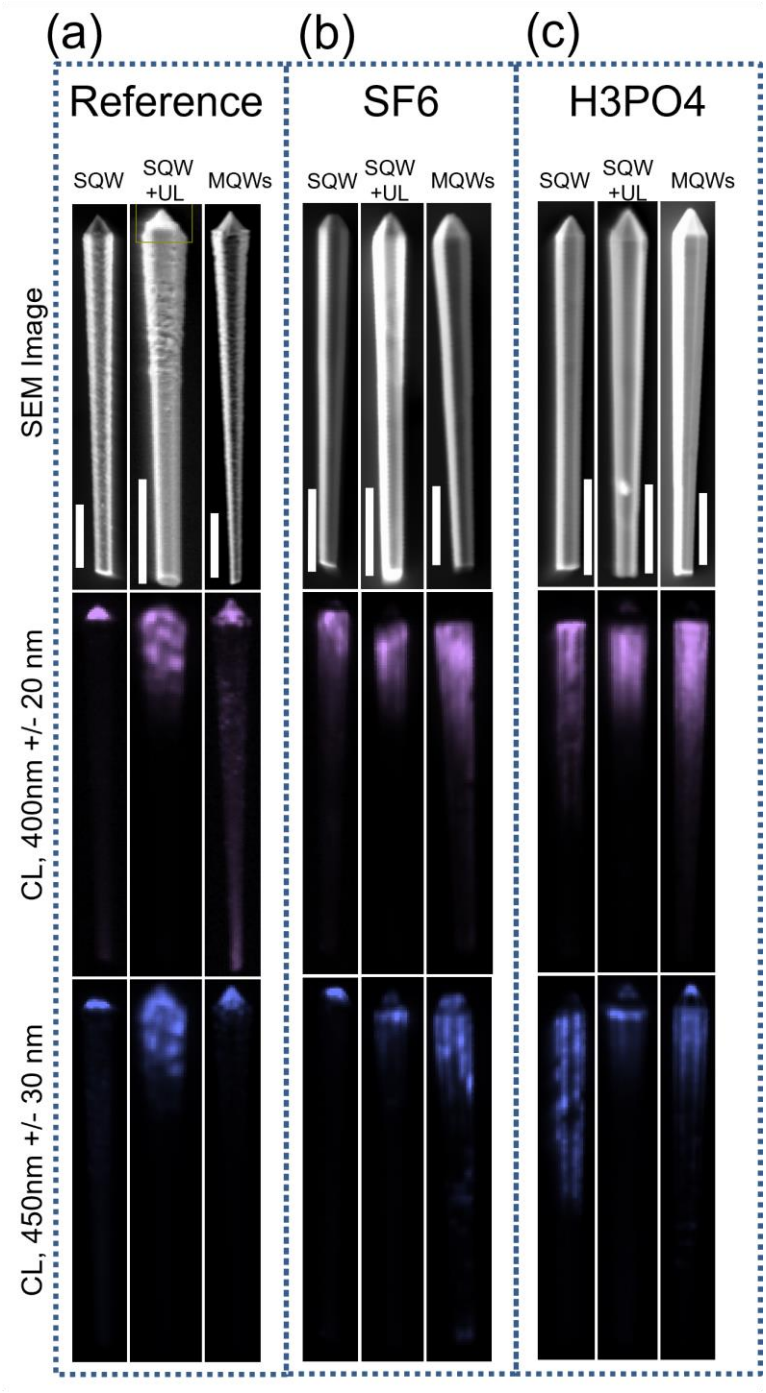

Figure 5. SEM image and CL maps at 400 and 450 nm for the reference sample (a), the SF_6 treated one (b) and the H_3PO_4 treated one (c). The scale bars are 2µm.

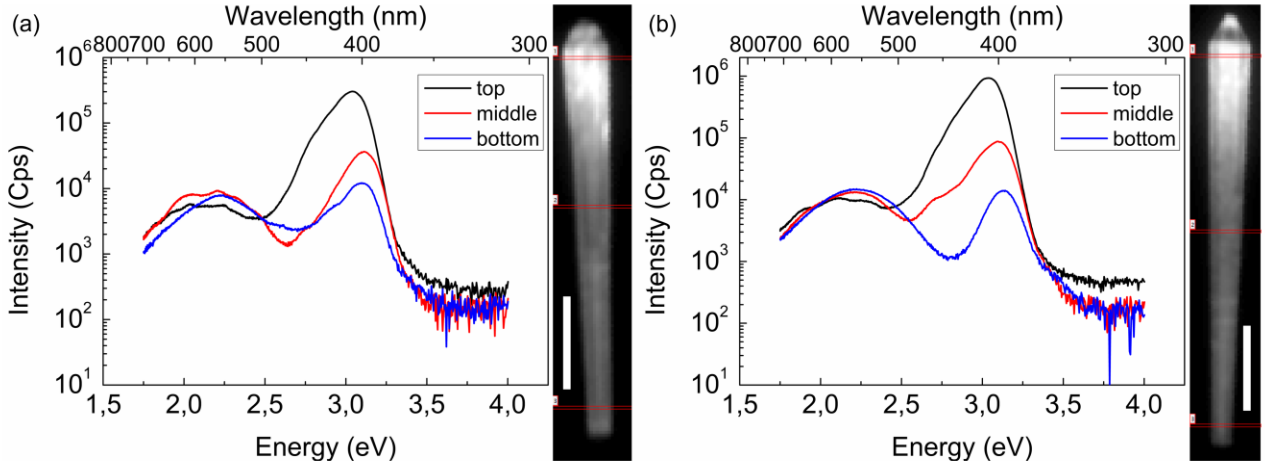

Figure 6. Room temperature CL spectra corresponding to the top, middle and bottom part of a SF_6 treated MQW sample (a) and a H_3PO_4 treated MQW sample (b). The scale bars are 2µm.

Type of shell		SQW	SQW+UL	MQW
Treatments	**No treatment**	Reference	Reference	Reference
	Chemical etching	BOE		
		KOH		
		H3PO4	H3PO4	H3PO4
	Dry etching	SF6	SF6	SF6
	In situ thermal etching	H2 annealing		

Table 1. Summary of the sample used for each process

ASSOCIATED CONTENT

SEM image of doped GaN nanowire etched in H_3PO_4 at 125°C for 15 minutes, showing a faster etching at the junctions between *m*-planes, additional SEM image of doped GaN nanowires annealed under H_2 at 1175°C for 15s at x15 000 and x50 000 magnification, and supplementary panchromatic, SEM, and color reconstitution of the SQW+UL reference sample with CL spectrum for three indicated points.

AUTHOR INFORMATION

Corresponding Author

*Julien Bosch: julien.bosch@crhea.cnrs.fr

Author Contributions

The manuscript was written through contributions of all authors. All authors have given approval to the final version of the manuscript.

Funding Sources

We acknowledge support from GANEX (ANR-11-LABX-0014). GANEX belongs to the public funded 'Investissements d'Avenir' program managed by the French ANR agency.

ACKNOWLEDGMENT

The authors would like to thank Mathieu Leroux for his fruitful discussions and precious advices

ABBREVIATIONS

LED, Light Emitting Diode; n-nid, doped/non intentionally doped; MOVPE, MetalOrganic Vapor Phase Epitaxy; QW, Quantum Well; QCSE, Quantum Confined Stark Effect; SAG,

Selective Area Growth; PECVD, Plasma Enhanced Vapor Phase Epitaxy; TMGa, Trimethylgallium; TMIn, Trimethylindium; BOE, Buffered Oxide Etch; ECR-RIE, Electron Cyclotron Resonance Reactive Ion Etching; SQW, Single Quantum Well; SQW+UL, Single Quantum Well + Underlayer; MQWs, Multi Quantum Well; UL, Underlayer; SEM, Scanning Electronic Microscope; CL,Cathodoluminescence; YB, Yellow Band

REFERENCES

(1) Arafin, S., Liu, X., & Mi, Z. (2013). Review of recent progress of III-nitride nanowire lasers. In Journal of Nanophotonics (Vol. 7, Issue 1, p. 074599). SPIE-Intl Soc Optical Eng. https://doi.org/10.1117/1.jnp.7.074599

(2) Johnson, J. C., Choi, H.-J., Knutsen, K. P., Schaller, R. D., Yang, P., & Saykally, R. J. (2002). Single gallium nitride nanowire lasers. In Nature Materials (Vol. 1, Issue 2, pp. 106–110). Springer Science and Business Media LLC. https://doi.org/10.1038/nmat728

(3) Li, S., & Waag, A. (2012). GaN based nanorods for solid state lighting. In Journal of Applied Physics (Vol. 111, Issue 7, p. 071101). AIP Publishing. https://doi.org/10.1063/1.3694674

(4) InGaN/GaN nanorod array white light-emitting diode. (2010). In Applied Physics Letters (Vol. 97, Issue 7, p. 073101). AIP Publishing. https://doi.org/10.1063/1.3478515

(5) Olivier, F., Tirano, S., Dupré, L., Aventurier, B., Largeron, C., & Templier, F. (2017). Influence of size-reduction on the performances of GaN-based micro-LEDs for display application. In Journal of Luminescence (Vol. 191, pp. 112–116). Elsevier BV. https://doi.org/10.1016/j.jlumin.2016.09.052

(6) Akasaki, I., Amano, H., Sota, S., Sakai, H., Tanaka, T., & Koike, M. (1995). Stimulated Emission by Current Injection from an AlGaN/GaN/GaInN Quantum Well Device. In Japanese Journal of Applied Physics (Vol. 34, Issue 11B, p. L1517). IOP Publishing. https://doi.org/10.7567/jjap.34.l1517

(7) Nakamura, S., Mukai, T., & Senoh, M. (1994). Candela-class high-brightness InGaN/AlGaN double-heterostructure blue-light-emitting diodes. In Applied Physics Letters (Vol. 64, Issue 13, pp. 1687–1689). AIP Publishing. https://doi.org/10.1063/1.111832

(8) Ren, C. X. (2016). Polarisation fields in III-nitrides: effects and control. In Materials Science and Technology (pp. 1–16). Informa UK Limited. https://doi.org/10.1179/1743284715y.0000000103

(9) Vennéguès, P., Beaumont, B., Bousquet, V., Vaille, M., & Gibart, P. (2000). Reduction mechanisms for defect densities in GaN using one- or two-step epitaxial lateral overgrowth methods. In Journal of Applied Physics (Vol. 87, Issue 9, pp. 4175–4181). AIP Publishing. https://doi.org/10.1063/1.373048

(10) Coulon, P. M., Mexis, M., Teisseire, M., Jublot, M., Vennéguès, P., Leroux, M., & Zuniga-Perez, J. (2014). Dual-polarity GaN micropillars grown by metalorganic vapour phase epitaxy: Cross-correlation between structural and optical properties. In Journal of Applied Physics (Vol. 115, Issue 15, p. 153504). AIP Publishing. https://doi.org/10.1063/1.4870950

(11) Hersee, S. D., Rishinaramangalam, A. K., Fairchild, M. N., Zhang, L., & Varangis, P. (2011). Threading defect elimination in GaN nanowires. In Journal of Materials Research (Vol. 26, Issue 17, pp. 2293–2298). Springer Science and Business Media LLC. https://doi.org/10.1557/jmr.2011.112

(12) Coulon, P.-M., Alloing, B., Brändli, V., Vennéguès, P., Leroux, M., & Zúñiga-Pérez, J. (2015). Dislocation filtering and polarity in the selective area growth of GaN nanowires by

continuous-flow metal organic vapor phase epitaxy. In Applied Physics Express (Vol. 9, Issue 1, p. 015502). IOP Publishing. https://doi.org/10.7567/apex.9.015502

(13) Coulon, P.-M., Vajargah, S. hosseini, Bao, A., Edwards, P. R., Le Boulbar, E. D., Girgel, I., Martin, R. W., Humphreys, C. J., Oliver, R. A., Allsopp, D. W. E., & Shields, P. A. (2017). Evolution of the m-Plane Quantum Well Morphology and Composition within a GaN/InGaN Core–Shell Structure. In Crystal Growth & Design (Vol. 17, Issue 2, pp. 474–482). American Chemical Society (ACS). https://doi.org/10.1021/acs.cgd.6b01281

(14) Kim, K.-C., Schmidt, M. C., Sato, H., Wu, F., Fellows, N., Jia, Z., Saito, M., Nakamura, S., DenBaars, S. P., Speck, J. S., & Fujito, K. (2007). Study of nonpolar m-plane InGaN/GaN multiquantum well light emitting diodes grown by homoepitaxial metal-organic chemical vapor deposition. In Applied Physics Letters (Vol. 91, Issue 18, p. 181120). AIP Publishing. https://doi.org/10.1063/1.2805029

(15) Hersee, S. D., Sun, X., & Wang, X. (2006). The Controlled Growth of GaN Nanowires. In Nano Letters (Vol. 6, Issue 8, pp. 1808–1811). American Chemical Society (ACS). https://doi.org/10.1021/nl060553t

(16) Jung, B. O., Bae, S.-Y., Kato, Y., Imura, M., Lee, D.-S., Honda, Y., & Amano, H. (2014). Morphology development of GaN nanowires using a pulsed-mode MOCVD growth technique. In CrystEngComm (Vol. 16, Issue 11, pp. 2273–2282). Royal Society of Chemistry (RSC). https://doi.org/10.1039/c3ce42266f

(17) Choi, K., Arita, M., & Arakawa, Y. (2012). Selective-area growth of thin GaN nanowires by MOCVD. In Journal of Crystal Growth (Vol. 357, pp. 58–61). Elsevier BV. https://doi.org/10.1016/j.jcrysgro.2012.07.025

(18) Coulon, P.-M., Alloing, B., Brändli, V., Lefebvre, D., Chenot, S., & Zúñiga-Pérez, J. (2015). Selective area growth of Ga-polar GaN nanowire arrays by continuous-flow MOVPE: A systematic study on the effect of growth conditions on the array properties. In physica status solidi (b) (Vol. 252, Issue 5, pp. 1096–1103). Wiley. https://doi.org/10.1002/pssb.201451589

(19) Tessarek, C., Bashouti, M., Heilmann, M., Dieker, C., Knoke, I., Spiecker, E., & Christiansen, S. (2013). Controlling morphology and optical properties of self-catalyzed, mask-free GaN rods and nanorods by metal-organic vapor phase epitaxy. In Journal of Applied Physics (Vol. 114, Issue 14, p. 144304). AIP Publishing. https://doi.org/10.1063/1.4824290

(20) Koester, R., Hwang, J. S., Durand, C., Le Si Dang, D., & Eymery, J. (2009). Self-assembled growth of catalyst-free GaN wires by metal–organic vapour phase epitaxy. In Nanotechnology (Vol. 21, Issue 1, p. 015602). IOP Publishing. https://doi.org/10.1088/0957-4484/21/1/015602

(21) Wang, X., Li, S., Mohajerani, M. S., Ledig, J., Wehmann, H.-H., Mandl, M., Strassburg, M., Steegmüller, U., Jahn, U., Lähnemann, J., Riechert, H., Griffiths, I., Cherns, D., & Waag, A. (2013). Continuous-Flow MOVPE of Ga-Polar GaN Column Arrays and Core–Shell LED Structures. In Crystal Growth & Design (Vol. 13, Issue 8, pp. 3475–3480). American Chemical Society (ACS). https://doi.org/10.1021/cg4003737

(22) Wang, X., Hartmann, J., Mandl, M., Sadat Mohajerani, M., Wehmann, H.-H., Strassburg, M., & Waag, A. (2014). Growth kinetics and mass transport mechanisms of GaN columns by

selective area metal organic vapor phase epitaxy. In Journal of Applied Physics (Vol. 115, Issue 16, p. 163104). AIP Publishing. https://doi.org/10.1063/1.4871782

(23) Hartmann, J., Wang, X., Schuhmann, H., Dziony, W., Caccamo, L., Ledig, J., Mohajerani, M. S., Schimpke, T., Bähr, M., Lilienkamp, G., Daum, W., Seibt, M., Straßburg, M., Wehmann, H.-H., & Waag, A. (2015). Growth mechanisms of GaN microrods for 3D core-shell LEDs: The influence of silane flow. In physica status solidi (a) (Vol. 212, Issue 12, pp. 2830–2836). Wiley. https://doi.org/10.1002/pssa.201532316

(24) Eymery, J.; Salomon, D.; Chen, X.; Durand, C. Process for Catalyst-Free Selective Growth on a Semiconductor Structure. Pat. WO/2012/136665, 2012

(25) Tessarek, C., Heilmann, M., Butzen, E., Haab, A., Hardtdegen, H., Dieker, C., Spiecker, E., & Christiansen, S. (2014). The Role of Si during the Growth of GaN Micro- and Nanorods. In Crystal Growth & Design (Vol. 14, Issue 3, pp. 1486–1492). American Chemical Society (ACS). https://doi.org/10.1021/cg500054w

(26) Tchoulfian, P., Donatini, F., Levy, F., Amstatt, B., Ferret, P., & Pernot, J. (2013). High conductivity in Si-doped GaN wires. In Applied Physics Letters (Vol. 102, Issue 12, p. 122116). AIP Publishing. https://doi.org/10.1063/1.4799167

(27) Tu, C.-G., Su, C.-Y., Liao, C.-H., Hsieh, C., Yao, Y.-F., Chen, H.-T., Lin, C.-H., Chen, H.-S., Kiang, Y.-W., & Yang, C. C. (2015). Regularly-patterned nanorod light-emitting diode arrays grown with metalorganic vapor-phase epitaxy. In Superlattices and Microstructures (Vol. 83, pp. 329–341). Elsevier BV. https://doi.org/10.1016/j.spmi.2015.03.050

(28) Grenier, V., Finot, S., Gayral, B., Bougerol, C., Jacopin, G., Eymery, J., & Durand, C. (2021). Toward Crack-Free Core–Shell GaN/AlGaN Quantum Wells. In Crystal Growth & Design (Vol. 21, Issue 11, pp. 6504–6511). American Chemical Society (ACS). https://doi.org/10.1021/acs.cgd.1c00943

(29) Deeb, M. A., Wei, J., Hartmann, J., Wehmann, H.-H., & Waag, A. (2015). Surface photovoltage behavior of GaN columns. In physica status solidi (a) (Vol. 212, Issue 4, pp. 732–735). Wiley. https://doi.org/10.1002/pssa.201400238

(30) Kapoor, A., Finot, S., Grenier, V., Robin, E., Bougerol, C., Bleuse, J., Jacopin, G., Eymery, J., & Durand, C. (2020). Role of Underlayer for Efficient Core–Shell InGaN QWs Grown on m-plane GaN Wire Sidewalls. In ACS Applied Materials & Interfaces (Vol. 12, Issue 16, pp. 19092–19101). American Chemical Society (ACS). https://doi.org/10.1021/acsami.9b19314

(31) Puchtler, T. J., Wang, T., Ren, C. X., Tang, F., Oliver, R. A., Taylor, R. A., & Zhu, T. (2016). Ultrafast, Polarized, Single-Photon Emission from m-Plane InGaN Quantum Dots on GaN Nanowires. In Nano Letters (Vol. 16, Issue 12, pp. 7779–7785). American Chemical Society (ACS). https://doi.org/10.1021/acs.nanolett.6b03980

(32) Tchernycheva, M., Neplokh, V., Zhang, H., Lavenus, P., Rigutti, L., Bayle, F., Julien, F. H., Babichev, A., Jacopin, G., Largeau, L., Ciechonski, R., Vescovi, G., & Kryliouk, O. (2015). Core–shell InGaN/GaN nanowire light emitting diodes analyzed by electron beam induced current microscopy and cathodoluminescence mapping. In Nanoscale (Vol. 7, Issue 27, pp. 11692–11701). Royal Society of Chemistry (RSC). https://doi.org/10.1039/c5nr00623f

(33) Zhang, H., Piazza, V., Neplokh, V., Guan, N., Bayle, F., Collin, S., Largeau, L., Babichev, A., Julien, F. H., & Tchernycheva, M. (2020). Correlated optical and electrical analyses of inhomogeneous core/shell InGaN/GaN nanowire light emitting diodes. In Nanotechnology (Vol. 32, Issue 10, p. 105202). IOP Publishing. https://doi.org/10.1088/1361-6528/abc70e

(34) Ren, C. X., Tang, F., Oliver, R. A., & Zhu, T. (2018). Nanoscopic insights into the effect of silicon on core-shell InGaN/GaN nanorods: Luminescence, composition, and structure. In Journal of Applied Physics (Vol. 123, Issue 4, p. 045103). AIP Publishing. https://doi.org/10.1063/1.5008363

(35) Tessarek, C., Rechberger, S., Dieker, C., Heilmann, M., Spiecker, E., & Christiansen, S. (2017). Understanding GaN/InGaN core–shell growth towards high quality factor whispering gallery modes from non-polar InGaN quantum wells on GaN rods. In Nanotechnology (Vol. 28, Issue 48, p. 485601). IOP Publishing. https://doi.org/10.1088/1361-6528/aa9050

(36) Finot, S., Grenier, V., Zubialevich, V., Bougerol, C., Pampili, P., Eymery, J., Parbrook, P. J., Durand, C., & Jacopin, G. (2020). Carrier dynamics near a crack in GaN microwires with AlGaN multiple quantum wells. In Applied Physics Letters (Vol. 117, Issue 22, p. 221105). AIP Publishing. https://doi.org/10.1063/5.0023545

(37) Rishinaramangalam, A. K., Nami, M., Shima, D. M., Balakrishnan, G., Brueck, S. R. J., & Feezell, D. F. (2016). Reduction of reverse-leakage current in selective-area-grown GaN-based core–shell nanostructure LEDs using AlGaN layers. In physica status solidi (a) (Vol. 214, Issue 5, p. 1600776). Wiley. https://doi.org/10.1002/pssa.201600776

(38) Nami, M., Rashidi, A., Monavarian, M., Mishkat-Ul-Masabih, S., Rishinaramangalam, Ashwin. K., Brueck, S. R. J., & Feezell, D. (2019). Electrically Injected GHz-Class GaN/InGaN Core–Shell Nanowire-Based μLEDs: Carrier Dynamics and Nanoscale Homogeneity. In ACS Photonics (Vol. 6, Issue 7, pp. 1618–1625). American Chemical Society (ACS). https://doi.org/10.1021/acsphotonics.9b00639

(39) Lu, W., Terazawa, M., Han, D.-P., Sone, N., Goto, N., Iida, K., Murakami, H., Iwaya, M., Tekeuchi, T., Kamiyama, S., & Akasaki, I. (2019). Structural and optical impacts of AlGaN undershells on coaxial GaInN/GaN multiple-quantum-shells nanowires. In Nanophotonics (Vol. 9, Issue 1, pp. 101–111). Walter de Gruyter GmbH. https://doi.org/10.1515/nanoph-2019-0328

(40) Lu, W., Sone, N., Goto, N., Iida, K., Suzuki, A., Han, D.-P., Iwaya, M., Tekeuchi, T., Kamiyama, S., & Akasaki, I. (2019). Effect of AlGaN undershell on the cathodoluminescence properties of coaxial GaInN/GaN multiple-quantum-shells nanowires. In Nanoscale (Vol. 11, Issue 40, pp. 18746–18757). Royal Society of Chemistry (RSC). https://doi.org/10.1039/c9nr07271c

(41) Schimpke, T., Lugauer, H.-J., Avramescu, A., Varghese, T., Koller, A., Hartmann, J., Ledig, J., Waag, A., & Strassburg, M. (2016). Position-controlled MOVPE growth and electro-optical characterization of core-shell InGaN/GaN microrod LEDs. (8 March 2016). Proc. SPIE 9768, Light-Emitting Diodes: Materials, Devices, and Applications for Solid State Lighting XX, 97680T https://doi.org/10.1117/12.2214122

(42) Coulon, P.-M., Damilano, B., Alloing, B., Chausse, P., Walde, S., Enslin, J., Armstrong, R., Vézian, S., Hagedorn, S., Wernicke, T., Massies, J., Zúñiga-Pérez, J., Weyers, M., Kneissl, M., & Shields, P. A. (2019). Displacement Talbot lithography for nano-engineering of III-nitride

materials. In Microsystems & Nanoengineering (Vol. 5, Issue 1). Springer Science and Business Media LLC. https://doi.org/10.1038/s41378-019-0101-2

(43) Wolf, R., Wandel, K., & Gruska, B. (2001). Low-temperature ICPECVD of silicon nitride in SiH4–NH3–Ar discharges analyzed by spectroscopic ellipsometry and etch behavior in KOH and BHF. In Surface and Coatings Technology (Vols. 142–144, pp. 786–791). Elsevier BV. https://doi.org/10.1016/s0257-8972(01)01184-7

(44) van Gelder, W., Hauser, V.E. (1967). The Etching of Silicon Nitride in Phosphoric Acid with Silicon Dioxide as a Mask. In J. Electrochem. Soc. (Volume 114, Issue 8, pp. 869-872). IOP Publishing

(45) Li, C., Wright, J. B., Liu, S., Lu, P., Figiel, J. J., Leung, B., Chow, W. W., Brener, I., Koleske, D. D., Luk, T.-S., Feezell, D. F., Brueck, S. R. J., & Wang, G. T. (2017). Nonpolar InGaN/GaN Core–Shell Single Nanowire Lasers. In Nano Letters (Vol. 17, Issue 2, pp. 1049–1055). American Chemical Society (ACS). https://doi.org/10.1021/acs.nanolett.6b04483

(46) Alloing, B., Vézian, S., Tottereau, O., Vennéguès, P., Beraudo, E., & Zuniga-Pérez, J. (2011). On the polarity of GaN micro- and nanowires epitaxially grown on sapphire (0001) and Si(111) substrates by metal organic vapor phase epitaxy and ammonia-molecular beam epitaxy. In Applied Physics Letters (Vol. 98, Issue 1, p. 011914). AIP Publishing. https://doi.org/10.1063/1.3525170

(47) Lai, Y.-Y., Hsu, S.-C., Chang, H.-S., Wu, Y. S., Chen, C.-H., Chen, L.-Y., & Cheng, Y.-J. (2016). The study of wet etching on GaN surface by potassium hydroxide solution. In Research

on Chemical Intermediates (Vol. 43, Issue 6, pp. 3563–3572). Springer Science and Business Media LLC. https://doi.org/10.1007/s11164-016-2430-1

(48) Stocker, D. A., Schubert, E. F., & Redwing, J. M. (1998). Crystallographic wet chemical etching of GaN. In Applied Physics Letters (Vol. 73, Issue 18, pp. 2654–2656). AIP Publishing. https://doi.org/10.1063/1.122543

(49) Shintani, A., & Minagawa, S. (1976). Etching of GaN Using Phosphoric Acid. In J. Electrochem. Soc. (Vol. 46, Issue 5, p.706-713). IOP Publishing

(50) Kazanowska, B. A., Sapkota, K. R., Lu, P., Talin, A. A., Bussmann, E., Ohta, T., Gunning, B. P., Jones, K. S., & Wang, G. T. (2021). Fabrication and field emission properties of vertical, tapered GaN nanowires etched via phosphoric acid. In Nanotechnology (Vol. 33, Issue 3, p. 035301). IOP Publishing. https://doi.org/10.1088/1361-6528/ac2981

(51) Maeng, J., Kwon, M.-K., Kwon, S.-S., Jo, G., Song, S., Kim, T.-W., Choi, B. S., Park, S.-J., & Lee, T. (2008). Comparison of Si Doping Effect on GaN Nanowires and Films Synthesized by Metal-Organic Chemical Vapor Deposition. In Journal of Nanoscience and Nanotechnology (Vol. 8, Issue 10, pp. 4934–4939). American Scientific Publishers. https://doi.org/10.1166/jnn.2008.1032

(52) Lee, S.-N., Paek, H. S., Son, J. K., Sakong, T., Nam, O. H., & Park, Y. (2007). Characteristics of Si and Mg doping in a-plane GaN grown on r-plane sapphire. In Journal of Crystal Growth (Vol. 307, Issue 2, pp. 358–362). Elsevier BV. https://doi.org/10.1016/j.jcrysgro.2007.07.027

(53) Molina, S. I., Sánchez, A. M., Pacheco, F. J., García, R., Sánchez-García, M. A., Sánchez, F. J., & Calleja, E. (1999). The effect of Si doping on the defect structure of GaN/AlN/Si(111). In Applied Physics Letters (Vol. 74, Issue 22, pp. 3362–3364). AIP Publishing. https://doi.org/10.1063/1.123345

(54) Chine, Z., Rebey, A., Touati, H., Goovaerts, E., Oueslati, M., Jani, B. E., & Laugt, S. (2006). Stress and density of defects in Si-doped GaN. In physica status solidi (a) (Vol. 203, Issue 8, pp. 1954–1961). Wiley. https://doi.org/10.1002/pssa.200521107

(55) Zhang, R., & Kuech, T. F. (1998). Photoluminescence of carbon in situ doped GaN grown by halide vapor phase epitaxy. In Applied Physics Letters (Vol. 72, Issue 13, pp. 1611–1613). AIP Publishing. https://doi.org/10.1063/1.121144

(56) Zhang, R., & Kuech, T. F. (1998). Hydrogen Induced Yellow Luminescence in GaN Grown by Halide Vapor Phase Epitaxy. In Journal of Electronic Materials (Vol. 27, Issue 5, pp. L35–L39). Springer Science and Business Media LLC. https://doi.org/10.1007/s11664-998-0185-1

(57) Kucheyev, S. O., Toth, M., Phillips, M. R., Williams, J. S., Jagadish, C., & Li, G. (2002). Chemical origin of the yellow luminescence in GaN. In Journal of Applied Physics (Vol. 91, Issue 9, pp. 5867–5874). AIP Publishing. https://doi.org/10.1063/1.1467605

(58) Gîrgel, I., Edwards, P. R., Le Boulbar, E., Coulon, P.-M., Sahonta, S.-L., Allsopp, D. W. E., Martin, R. W., Humphreys, C. J., & Shields, P. A. (2016). Investigation of indium gallium nitride facet-dependent nonpolar growth rates and composition for core–shell light-emitting diodes. In Journal of Nanophotonics (Vol. 10, Issue 1, p. 016010). SPIE-Intl Soc Optical Eng. https://doi.org/10.1117/1.jnp.10.016010

(59) Lu, P. F., Sun, C., Cao, H. W., Ye, H., Zhong, X. X., Yu, Z. Y., Han, L. H., & Wang, S. M. (2014). Strain induced composition profile in InGaN/GaN core–shell nanowires. In Solid State Communications (Vol. 178, pp. 1–6). Elsevier BV. https://doi.org/10.1016/j.ssc.2013.10.011

(60) Griffiths, J. T., Ren, C. X., Coulon, P.-M., Le Boulbar, E. D., Bryce, C. G., Girgel, I., Howkins, A., Boyd, I., Martin, R. W., Allsopp, D. W. E., Shields, P. A., Humphreys, C. J., & Oliver, R. A. (2017). Structural impact on the nanoscale optical properties of InGaN core-shell nanorods. In Applied Physics Letters (Vol. 110, Issue 17, p. 172105). AIP Publishing. https://doi.org/10.1063/1.4982594

(61) Schmidt, G., Müller, M., Veit, P., Metzner, S., Bertram, F., Hartmann, J., Zhou, H., Wehmann, H.-H., Waag, A., & Christen, J. (2018). Direct imaging of Indium-rich triangular nanoprisms self-organized formed at the edges of InGaN/GaN core-shell nanorods. In Scientific Reports (Vol. 8, Issue 1). Springer Science and Business Media LLC. https://doi.org/10.1038/s41598-018-34382-y

(62) Haller, C., Carlin, J.-F., Jacopin, G., Liu, W., Martin, D., Butté, R., & Grandjean, N. (2018). GaN surface as the source of non-radiative defects in InGaN/GaN quantum wells. In Applied Physics Letters (Vol. 113, Issue 11, p. 111106). AIP Publishing. https://doi.org/10.1063/1.5048010

(63) Akasaka, T., Gotoh, H., Saito, T., & Makimoto, T. (2004). High luminescent efficiency of InGaN multiple quantum wells grown on InGaN underlying layers. In Applied Physics Letters (Vol. 85, Issue 15, pp. 3089–3091). AIP Publishing. https://doi.org/10.1063/1.1804607

(64) Armstrong, A., Henry, T. A., Koleske, D. D., Crawford, M. H., & Lee, S. R. (2012). Quantitative and depth-resolved deep level defect distributions in InGaN/GaN light emitting diodes. In Optics Express (Vol. 20, Issue S6, p. A812). The Optical Society. https://doi.org/10.1364/oe.20.00a812

(65) Zubialevich, V. Z., Pampili, P., & Parbrook, P. J. (2020). Thermal Stability of Crystallographic Planes of GaN Nanocolumns and Their Overgrowth by Metal Organic Vapor Phase Epitaxy. In Crystal Growth & Design (Vol. 20, Issue 6, pp. 3686–3700). American Chemical Society (ACS). https://doi.org/10.1021/acs.cgd.9b01656

For Table of Contents Use Only

Manuscript title: Etching of the SiGaNx passivation layer for full emissive lateral facet coverage in InGaN/GaN core-shell nanowires by MOVPE

Authors: Julien Bosch, Pierre-Marie Coulon, Sébastien Chenot, Marc Portail, Christophe Durand, Maria Tchernycheva, Philip A Shields, Jesús Zúñiga-Pérez, Blandine Alloing

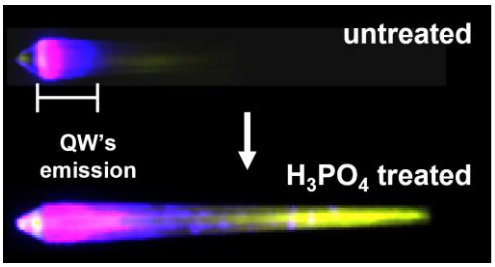

Cathodoluminescence mapping showing the evolution of the true color emission of an InGaN structure with no treatment between core and shell growth, and with an H_3PO_4 treatment